Geoderma 432 (2023) 116419

Contents lists available at ScienceDirect

Geoderma

journal homepage: www.elsevier.com/locate/geoderma

Relationship between thermal and electrical conductivity curves of soils with a unimodal pore size distribution: Part 2. Estimating bulk electrical conductivity from thermal conductivity

Weiliu Li [a], Lin Liu [a], Yili Lu [a], Tusheng Ren [a,*], Robert Horton [b]

[a] College of Land Science and Technology, China Agricultural University, Beijing 100193, China
[b] Agronomy Department, Iowa State University, Ames, IA 50011, USA

ARTICLE INFO

Handling Editor: Morgan Cristine L.S.

Keywords:
Electrical conductivity
Thermal conductivity
Soil texture
Bulk density
Water content
Model

ABSTRACT

Soil thermal conductivity (λ) and electrical conductivity (σ) influence heat conduction and electrical conduction through soils. In Part 1 of this two-part series, we demonstrated that for soils with a unimodal pore size distribution, the λ and σ curves were interrelated and could be described with a unified series–parallel resistor model. Based on the conceptual model presented in Part 1, the "mirror image" phenomenon in the λ-σ relationship was further evaluated. Starting with the Lu et al. (2007) λ model, the "mirror image" phenomenon was used to derive a new normalized σ model. The new σ model was dependent on degree of water saturation (*S*), and shared the same shape parameters as those in the λ model. Here, the new σ model is examined using new datasets consisting of simultaneous thermo-TDR sensor measurements of soil water content (θ), λ and σ. New model σ values interpolated between known dry and saturated σ values agreed well with measured σ values, with RMSE values within 0.102 dS m^{-1} and bias values between −0.083 and 0.014 dS m^{-1} for a variety of soil samples. Using repeated in situ λ measurements made in soils during an evaporative drying period, the new σ model estimated normalized σ values with RMSEs within 0.015 dS m^{-1}. The new σ model offers an effective way to estimate σ of unsaturated soils.

1. Introduction

The bulk soil electrical conductivity (σ) denotes the capability of a soil to conduct electricity. Values of σ have been used extensively to estimate other soil parameter values, e.g., water content (θ), degree of saturation (*S*), mineralogy, salinity, and clay content (Myers et al., 2007; Martinez et al., 2009; Stadler et al., 2015; Nocco et al., 2018). Knowledge of σ has enabled the tracking of soil nutrient status, thus acting as a guide to schedule irrigation and fertilization (Rhoades and Loveday, 1990; Kitchen et al., 1999; Corwin and Lesch, 2005). Accurate σ determinations are useful for understanding spatial and temporal distribution of various soil parameters at the field scale.

Soil σ varies with texture, mineral composition, bulk density, water content, and temperature. Several studies have focused on monitoring and modeling σ dynamics in situ. Ground penetrating radar and time domain reflectometry are widely used to map σ and related variables at the field scale (Brovelli and Cassiani, 2011; Doolittle and Brevik, 2014). Several theoretical and empirical models have been developed to estimate σ (Gupta and Hanks, 1972; Rhoades et al., 1976; Mualem and Friedman, 1991; Ewing and Hunt, 2006; Fu et al., 2021), mainly for sandy and stony soils. Among these, Archie's law is applied widely in rocks and sandy soils to describe σ as an exponential function of porosity (Archie, 1942; Keller, 1994). Fu et al. (2021) developed a general form of Archie's law to estimate σ of unsaturated soils, using the known dry and saturated σ values.

The electrical conductivity of fine-textured soils is enhanced due to the large number of ions adsorbed to clay minerals (Hendrickx et al., 2002). Rhoades et al. (1976) developed a simple physical model by assuming that σ was the integrated result of two parallel conductors, i.e., the bulk liquid-phase conductivity (due to free salt in the liquid-filled pores) and the bulk surface conductivity (due to exchangeable ions at the solid/liquid interface). The contribution of soil air to electrical conductivity was neglected. Later, Rhoades et al. (1989) improved this model by considering electrical conduction through three paths acting in parallel, including a solid pathway, a liquid pathway, and a solid-water series-coupled pathway for soil conditions of low solute concentration

* Corresponding author.
E-mail address: tsren@cau.edu.cn (T. Ren).

https://doi.org/10.1016/j.geoderma.2023.116419
Received 26 November 2022; Received in revised form 28 February 2023; Accepted 1 March 2023
Available online 7 March 2023

and θ values. Numerical models have also been developed to estimate the bulk electrical conductivity of rocks and soils (Tabbagh et al., 2002; Tang et al., 2015). Cai et al. (2017) provide a review of electrical conduction mechanisms in porous media and of σ models for saturated soil conditions.

It is recognized that electrical conduction, heat transfer, and water flow are all affected by a number of common factors, such as θ, bulk density (ρ_b), mineral composition, temperature, and particle size distribution (Nadler and Frenkel, 1980; Farouki, 1986; Bai et al., 2013; Corwin and Lesch, 2005; Logsdon et al., 2010; Lu et al., 2014; Tong et al., 2015; Bertermann and Schwarz, 2017). Inspired by similarities between electrical conduction, heat transfer, and water flow in soils, studies have been performed to understand interrelations between σ, soil thermal conductivity (λ), and hydraulic conductivity (K_s). Mualem and Friedman (1991) developed a conceptual σ model with inclusion of ion mobility, and further proposed an equation describing the relationship between σ and K_s. Studies have addressed similarities between λ and σ, and simple λ-σ models were proposed for use on specific soils (Globus and Arefyev, 1975; Gerayzade et al., 1987; Singh et al., 2001; Sreedeep et al., 2005; Fragkogiannis et al., 2010; Tokoro et al., 2016; Wang et al., 2017; Sun and Lv, 2019). In Part 1 of this two-part series, we presented a unified series–parallel resistor model that described the λ(θ) and σ(θ) curves by considering three conduction pathways for heat and electricity. Although λ and σ behaved differently in the hydration, menisci, and continuous liquid regions, there existed a "mirror image" phenomenon between the normalized λ(θ) curve and the σ(θ) curve, which provided an opportunity to estimate one of the curves from the other (Tokoro et al., 2016).

It is a challenge to measure σ, λ, and K_s simultaneously for the same soil volume. Thus, physically-based σ models have only been tested on the limited number of available datasets, especially datasets representing field conditions. Likewise, specific calibration is usually necessary for empirical models to achieve the required accuracy. The thermo-TDR technique, which measures in situ θ, λ, and σ values simultaneously for a similar soil volume (Ren et al., 1999; Peng et al., 2019), provides an opportunity to obtain comprehensive datasets for a range of water content and bulk density values.

In this study, we introduce a new model to estimate σ(θ) curves from measured λ(θ) curves for soils with a unimodal pore size distribution. The model was validated using thermo-TDR sensor measurements of λ and σ as functions of θ.

2. Model development

We employed the normalized λ model of Lu et al. (2007) to derive a new σ model based on the σ-λ "mirror image" analogy illustrated in Part 1 of this two-part series. While it has been extensively tested and validated in different soils and under various conditions, this model has a simple form so that the σ -*S* relation can be easily expressed as the inverse function of the λ-*S* model. The Lu et al. (2007) λ model includes three factors (soil texture, ρ_b and θ) and two parameters (*B* and *C*). The normalized form is expressed as,

$$K_e(\lambda) = \frac{\lambda - \lambda_{dry}}{\lambda_{sat} - \lambda_{dry}} = \exp\left\{B\left[1 - S^{(B-C)}\right]\right\} \quad (1)$$

where $K_e(\lambda)$ is the normalized thermal conductivity, λ_{dry} and λ_{sat} represent the thermal conductivities of dry and saturated soils, *B* is a soil texture dependent parameter, and *C* is a shape parameter with a value of 1.33. *B* has a value of 0.96 for soils with sand content greater than 40%, and a value of 0.27 for other soils.

Lu et al. (2007) introduced the following formula to estimate dry soil λ values,

$$\lambda_{dry} = -0.56n + 0.51 \quad (2)$$

where *n* is total porosity ranging from 0.20 and 0.60.

For saturated soils, λ values (λ_{sat}) are calculated as (Johansen, 1975),

$$\lambda_{sat} = \lambda_s^{1-n}\lambda_w^n \quad (3)$$

where λ_w is the thermal conductivity of pure water, which is 0.594 W m^{-1} K^{-1} at 20 °C, λ_s is the thermal conductivity of soil solids, which is estimated as,

$$\lambda_s = \lambda_o^{1-q}\lambda_q^q \quad (4)$$

where *q* represents the quartz fraction of the soil solids. The thermal conductivity of quartz, λ_q, is taken as 7.7 W m^{-1} K^{-1}. The thermal conductivity of other minerals, λ_o, is taken as 2.0 W m^{-1} K^{-1} when $q > 0.2$, and 3.0 W m^{-1} K^{-1} when $q \leq 0.2$, respectively.

Finally, λ is calculated with Eq. (5),

$$\lambda = (\lambda_{sat} - \lambda_{dry})K_e(\lambda) + \lambda_{dry} \quad (5)$$

In Part 1 of this two-part series, we partitioned the λ(θ) and σ(θ) curves into three sections by considering the interaction of water with soil solids. In Section I, soil water is adsorbed onto solid particle surfaces and electrical current and heat conduction occur only via the solid-to-solid pathway. As water bridges form among solid particles (Section II), the formation of a solid–liquid-solid pathway improves heat conduction, which results in a dramatic λ increase with θ. At this stage, however, the expansion of electrical conduction (i.e., σ change with θ) is relatively slow. In the continuous liquid pathway (Section III), a surge of σ in response to θ increase is observed while the rate of λ increases slow as compared to that in Section II. Our analysis indicated a "mirror image" relationship between the $K_e(\lambda)$-*S* and $K_e(\sigma)$-*S* curves in Sections II and III. Thus, in Sections II and III, it is reasonable to hypothesize that the λ(θ) and σ(θ) curves are symmetrical about line $y = x$ and the normalized λ and σ (i.e., $K_e(\lambda)$ and $K_e(\sigma)$) are related inversely.

The inverse function of Eq. (1) is,

$$S = \exp\left\{B\left[1 - K_e(\sigma)^{(B-C)}\right]\right\} \quad (6)$$

where *S* is determined with ρ_b and θ, and *B* and *C* are the parameters defined previously in the Lu et al. (2007) λ model.

Thus, the is expressed as,

$$K_e(\sigma) = \left(1 - \frac{\ln S}{B}\right)^{\frac{1}{B-C}} \quad (7)$$

If the dry and saturated soil σ values (i.e., σ_{sat} and σ_{dry}) are measured, the σ values at other *S* values can be estimated with the following equation,

$$\sigma = (\sigma_{sat} - \sigma_{dry})K_e(\sigma) + \sigma_{dry} \quad (8)$$

Table 1
Selected properties of the soils used in this study.

Soil ID	Texture	Particle size distribution			Organic matter content	Particle density
		2–0.05 mm	0.05–0.002 mm	<0.002 mm		
		g g^{-1}			%	Mg m^{-3}
1	sand	0.91	0.03	0.06	0.09	2.66
2	silt loam	0.34	0.53	0.13	0.24	2.67
3	sandy loam	0.52	0.36	0.12	0.74	2.65
4	sand	0.94	0.01	0.05	0.09	2.65
5	sandy loam	0.39	0.60	0.01	0.75	2.65
6	silt loam	0.50	0.41	0.09	0.25	2.65

3. Materials and methods

We performed two independent experiments on 6 soils (Soils 1–6, with textures ranging from sand to silt loam, Table 1), to determine the changes of λ and σ as a function of θ. The data were then used to evaluate the model performance. The soil samples were air-dried, ground, and sieved through a 2-mm screen for the pre-treatment. Soil particle size distributions were determined with the pipette method (Gee and Or, 2002). Soil organic matter contents were determined using the Walkely-Black titration method (Nelson and Sommers, 1996). Soil particle densities were determined with the pycnometer method (Flint and Flint, 2002).

3.1. Simultaneous measurements of θ, λ, and σ with a thermo-TDR sensor

A thermo-TDR sensor, with 45-mm probe length, 2-mm probe diameter and 8-mm probe spacing, was used to simultaneously measure θ, λ and σ of the repacked soil samples (Ren et al., 1999). For heat pulse measurements, a constant current (~0.17 A) was introduced into the central heater probe (with the resistance of 888 Ω m^{-1}) for a short time duration of 8–15 s. The temperature-change with time data in the two outer probes were measured at a 1-s interval for 300 s after initiating a heat pulse. The heat pulse durations were regulated to make sure the temperature-change with time data had maximum values in the range of 0.5–0.9 °C to minimize water and vapor redistributions induced by the heat input. Control of the heat pulse and recording of temperature data were performed with a datalogger (model CR3000, Campbell Scientific, Logan, UT). Finally, soil λ values were determined by fitting the identical cylindrical perfect conductors (ICPC) theory to the measured temperature-rise data (Knight et al., 2012; Lu et al., 2013). Details about thermo-TDR theory and measurements can be found in Lu et al. (2017).

To obtain TDR measurements, the thermo-TDR sensor was connected to a TDR100 reflectometer device (Campbell Scientific, Logan, UT), and the TDR waveforms were automatically obtained to calculate the θ and σ. To determine θ, soil dielectric constant was obtained from the first and second reflection points of the TDR waveforms collected with the datalogger, and θ was estimated by using the Topp et al. (1980) equation.

The following equation was used to calculate σ,

$$\sigma = \frac{K_p}{R_s} f_T \tag{9}$$

where K_p is the geometric constant of the thermo-TDR sensor used in this study (m^{-1}), f_T is the temperature correction factor, and R_s is the impedance of the sample (Ω).

For comparison purposes, all of the σ values were converted from the observed temperature, T, condition to a reference temperature condition of 25 °C using (Heimovaara et al., 1995),

$$f_T = \frac{1}{1 + 0.0191(T - 25)} \tag{10}$$

Parameter R_s was obtained following the procedure of Heimovaara et al. (1995),

$$R_s = R_t - R_{cable} \tag{11}$$

where R_t is the total impedance of the cable tester, coaxial cable, and sensor inserted in a sample (Ω), R_{cable} represents the combined series impedance in the cable, connectors, and cable tester (Heimovaara et al., 1995), which is determined directly from the TDR waveforms using,

$$R_t = Z_c \frac{1 + \rho_\infty}{1 - \rho_\infty} \tag{12}$$

where Z_c is the impedance of the coaxial cable (75 Ω), ρ_∞ is the reflection coefficient at a distant point from the first reflection on a waveform,

$$\rho_\infty = \frac{v_\infty - v_0}{v_0} \tag{13}$$

where v_∞ and v_0 are the signal amplitude at the distance point and the TDR instrument, respectively (Heimovaara et al., 1995).

Before making σ and θ measurements, the thermo-TDR sensor was calibrated to obtain K_p, R_{cable}, and probe length. K_p and R_{cable} were calibrated in a series of KCl solutions with different concentrations of known σ values. The reflection points on the TDR waveform, which are used to determine the dielectric constant of the soil sample, are sensitive to errors in probe length. In this study, we calibrated the probe length by analyzing the TDR waveforms in distilled water with a known dielectric constant (80 at 25 °C).The K_p, R_{cable} and length of the sensor were 4.45 m^{-1}, 76.08 Ω and 45 mm, respectively.

3.2. Experiment 1: Discrete measurements at selected values of water content and bulk density

First, θ, λ, and σ measurements were made on soils 1, 2, and 3 at desired ρ_b and θ values. The soil samples were repacked into cylinders (50-mm inner diameter and 50-mm high) in a temperature regulated room (25 ± 1 °C). For soil 1, θ values were 0.00, 0.05, 0.10, 0.15 and 0.20 m^3 m^{-3} at ρ_b values of 1.40, 1.50 and 1.60 Mg m^{-3}. For soil 2, the designated θ values were 0.00, 0.05, 0.10, 0.15, 0.20, 0.25, and 0.30 m^3 m^{-3}, at ρ_b values of 1.15, 1.25, and 1.35 Mg m^{-3}. Soil 3 had the same θ values used for soil 2, but the ρ_b values were 1.25, 1.35, and 1.45 Mg m^{-3} (Table 2). Three replicated soil columns were prepared for each θ and ρ_b combination. The repacked soil cores were tightly sealed (to avoid any water loss) and placed in a temperature-regulated room (25 °C ± 1) for 12 h before making thermo-TDR measurements.

To determine the θ, λ, and σ of each sample, a thermo-TDR sensor was inserted into the soil column vertically from the soil surface, and heat-pulse and TDR measurements were performed following the procedures described in section 3.1. At the end, the soil cores were oven-dried at 105 °C for 24 h to directly determine θ and ρ_b values.

3.3. Experiment 2: Repeated thermo-TDR measurements with time during a drying period

In Experiment 1, the λ and σ data were obtained on individual soil cores. No observations were made in nearly saturated soils because of the difficulty to pack wet soil uniformly. To investigate λ and σ as affected by θ for nearly-saturated soil, an evaporation experiment was performed on initially wet soils 4–6. Soil samples were packed into

Table 2
The input parameters used in the new soil electrical conductivity (σ) model. σ_{dry} and σ_{sat} represent the bulk soil electrical conductivity values for dry and saturated soil conditions, respectively; λ_{dry} and λ_{sat} represent the soil thermal conductivity values for dry and saturated soil conditions, respectively.

Soil ID	Texture	Parameter B in Eq. (7)	Bulk density	σ_{dry}	σ_{sat}	λ_{dry}	λ_{sat}
			Mg m^{-3}	dS m^{-1}		W m^{-1} K^{-1}	
1	sand	0.96	1.40	0.08	0.20	0.27	2.16
			1.50	0.09	0.23	0.28	2.34
			1.60	0.08	0.26	0.30	2.62
2	silt loam	0.27	1.15	0.09	1.05	0.23	1.24
			1.25	0.09	0.97	0.26	1.32
			1.35	0.09	0.93	0.29	1.42
3	sandy loam	0.96	1.25	0.09	0.89	0.25	1.48
			1.35	0.08	0.85	0.28	1.58
			1.45	0.09	0.82	0.29	1.71
4	sand	0.96	1.75	0.06	0.23	–	–
5	sandy loam	0.27	1.53	0.08	0.40	–	–
6	silt loam	0.96	1.36	0.07	0.40	–	–

cylinders (80-mm inner diameter and 90-mm high) at a θ of 0.30 m^3 m^{-3}, and ρ_b values of 1.75, 1.53, and 1.36 Mg m^{-3} for soils 4, 5, and 6, respectively (Table 2). A thermo-TDR sensor was inserted into the cylinder from a pre-drilled hole (positioned horizontally with respect to the soil surface) at the depth of 4.5 cm. Each soil core was slowly saturated with water, and then allowed to dry gradually by exposing the open top surface to the atmosphere. During the drying process, repeated θ, λ, and σ measurements in time were made with a thermo-TDR sensor. Lu et al. (2019) used a similar experiment setup to obtain soil λ and matric suction data during soil drying. The thermo-TDR measurements were made hourly over the drying period until there were no further decreases in the TDR measured θ values. Finally, θ and ρ_b values were determined directly by oven drying each soil core to constant mass at 105 °C.

We also determined the thermal and electrical conductivity values of dry and saturated soil samples. For each of the soils (soils 4–6), two dry core samples (50-mm inner diameter and 50-mm high) were prepared at the specified bulk density. One core sample of each soil was placed in a container and slowly saturated with distilled water until water films appeared at the soil surface. The height of distilled water in the container was about half of the cylinder length. A thermo-TDR sensor was used to measure the σ_{sat}, σ_{dry}, λ_{sat}, and λ_{dry} values. Following the thermo-TDR measurements, the soil cores were oven-dried at 105 °C for 24 h to directly determine the θ and ρ_b values.

3.4. Model evaluation

We evaluated the new model's ability to estimate σ by using root mean square error (RMSE) and bias of the estimate,

$$RMSE = \sqrt{\frac{\sum (A_i - A_j)^2}{n}} \quad (14)$$

$$bias = \frac{\sum (A_i - A_j)}{n} \quad (15)$$

where n is the number of measurements, A_i is the measured value, and A_j is the model estimated value.

4. Results and discussion

Fig. 1 presents comparisons of measured and Lu et al. (2007) model estimated λ values as a function of water content at various ρ_b values for soils 1, 2, and 3. The thermo-TDR measured λ_{dry} and λ_{sat} values are listed in Table 2. Overall, the measured and estimated λ values agreed well with RMSEs ranging from 0.032 to 0.058 W m^{-1} K^{-1}. It is apparent that the Lu et al. (2007) model not only captured the trend of λ as responses to θ in the three heat conduction regimes, but also accurately described the influences of texture, ρ_b and θ on λ.

Fig. 2 presents comparisons of new model-estimated σ values versus thermo-TDR measured values at specified ρ_b values for soils 1–3. The thermo-TDR measured σ_{dry} and σ_{sat} values (Table 2, grey dots in Fig. 2) were used in the model (i.e., Eq. (8)). For the 6 soils, the σ_{dry} values varied over a narrow range of 0.06–0.09 dS m^{-1}, while the σ_{sat} values ranged from 0.20 to 1.05 dS m^{-1}, depending mainly on the solute concentration in soil solutions. Except for soil 5, the σ_{sat} values increased linearly with soil clay content (data not shown). The accuracies of the new σ interpolation model for unsaturated conditions, as expressed by RMSE and bias values, are presented in Table 3. The RMSEs of σ estimates were within 0.111 dS m^{-1}, and the bias values of σ estimates were in the range of −0.101 to 0.014 dS m^{-1}, indicating that the new model performed well over a range of ρ_b and θ values for these soils. Consistent agreement existed for the modeled and measured σ values for soils 1 and 3 (sandy soils), while on soil 2 (a silt loam), the new model overestimated σ at low and intermediate θ values (Fig. 2(d), 2(e), 2(f)).

The model estimate errors in soil 2 arose in part because the underpinning unified series–parallel resistor model was built on the assumption that investigated soils have a unimodal pore size distribution. The assumption is reasonable for poorly aggregated soils (e.g., soils 1 and 3) that have a well-graded pore system. For strongly aggregated soils (e.g., soil 2), most solid particles are bound together to form aggregates, which forms a dual-porosity structure, i.e., the pore system consists of inter-aggregate pores and intra-aggregate pores (Satyanaga et al., 2013). When the soil is wetted, water first enters the intra-aggregate pores (micropores), followed by the smaller interaggregate pores, and then the larger interaggregate pores (macropores), which deviates from the theory of the unified series–parallel resistor model. Thus, the "mirror image" relationship between the normalized thermal and electrical conductivity, which is developed on the assumption that the soil has a unimodal pore size distribution, may not fully apply to the soils with a bimodal pore size distribution. Further studies are required to understand the relationship between normalized thermal and electrical conductivity on soils with bimodal pore size distributions.

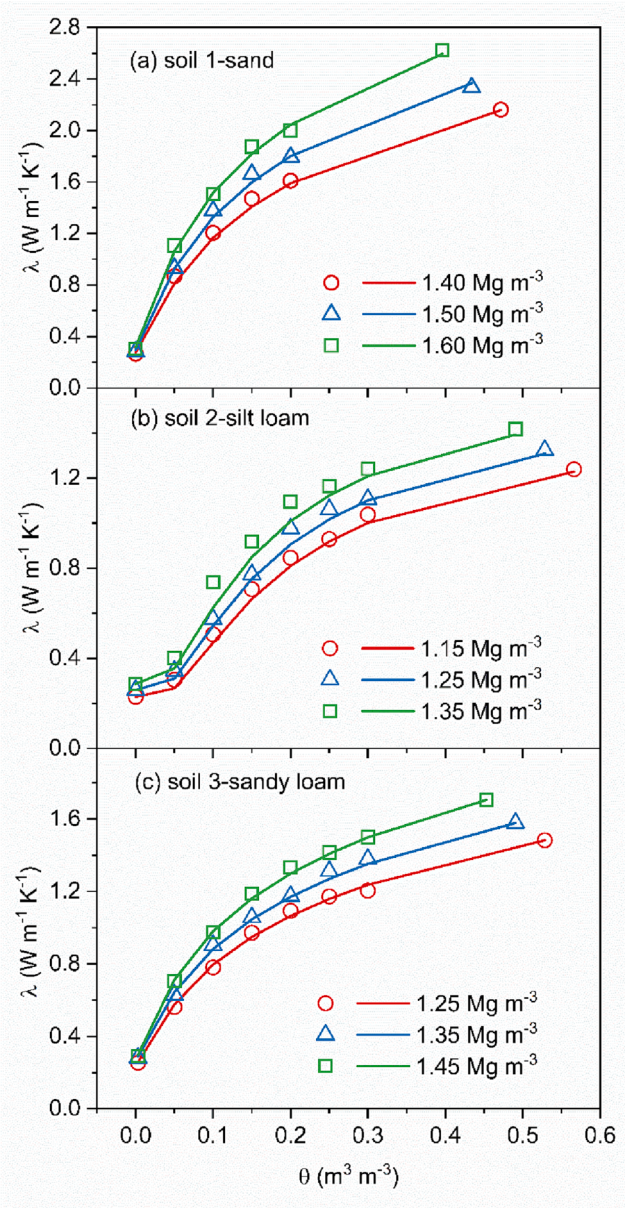

Fig. 1. The measured (symbols) and the Lu et al. (2007) model estimated (curves) soil thermal conductivity (λ) values vs. water content (θ) for selected bulk density values of soils 1–3.

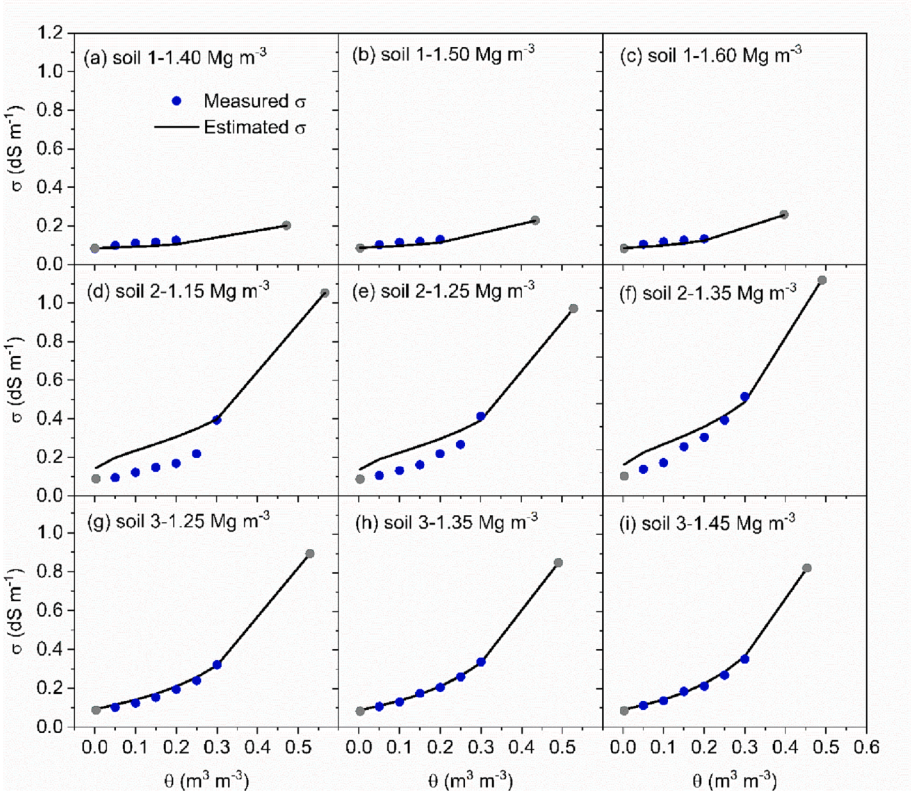

Fig. 2. The measured (symbols) and the new model estimated (curves) soil electrical conductivity (σ) values versus water content (θ) at selected bulk density (ρ_b) for soils 1–3. The grey dots represent dry and saturated soil conditions.

Table 3
The root mean square error (RMSE) and bias of bulk soil electrical conductivity values estimated with the new model.

Soil ID	Texture	Bulk density	RMSE	bias
		Mg m^{-3}	dS m^{-1}	
1	sand	1.40	0.016	0.014
		1.50	0.013	0.012
		1.60	0.013	0.012
2	silt loam	1.15	0.111	−0.101
		1.25	0.078	−0.067
		1.35	0.053	−0.040
3	sandy loam	1.25	0.015	−0.013
		1.35	0.005	−0.002
		1.45	0.011	−0.008
4	sand	1.75	0.007	0.000
5	sandy loam	1.53	0.015	−0.010
6	silt loam	1.36	0.012	0.005

Fig. 3 compares the measured and the estimated $K_e(\sigma)$ values obtained on soils 4–6 during the drying process. The measured and estimated $K_e(\sigma)$ values generally distributed along the 1:1 line, the slopes of the regression lines were close to unity, and the coefficients of determination were greater than 0.98. We further estimated σ values with Eq. (8) by using the thermo-TDR measured σ_{dry} and σ_{sat} values for soils 4–6. The RMSEs of the σ estimates were within 0.015 dS m^{-1}, and the biases of estimated data were less than 0.005 dS m^{-1} (Table 3). Therefore, the new model not only well captured $K_e(\sigma)$ as a function of S, but also provided accurate σ data. These results also imply the potential to estimate in situ soil thermal conductivity from bulk electrical conductivity measurements, which is especially important at field and regional scales.

It is noteworthy that the unified series–parallel model (as described in Part 1 of this two-part series) was developed using natural soils with a σ range of 0–1.2 dS m^{-1}, while the bulk electrical conductivity model introduced here was tested only in the σ range of 0.06–1.05 dS m^{-1}. Measurements indicated that soil salinity greatly affected σ but had little effect on λ values (Peng et al., 2022). Further studies are required to investigate the relationship between $K_e(\lambda)$ and $K_e(\sigma)$ on high salinity soils, and to quantify the effect of soil salinity on the performance of the new σ model.

5. Conclusions

In this study, the changes of λ(θ) and σ(θ) functions were quantified and analyzed, and a new model was developed to estimate σ from easily measured variables. In Part 1 of this two-part series, a unified series–parallel model for soils with unimodal pore size distributions was developed to describe the λ(θ) and σ(θ) curves by considering solid, solid–liquid, and liquid pathways with respect to three θ ranges that had distinct characteristics. A "mirror image" phenomenon between the normalized thermal conductivity and electrical conductivity curves (i.e., between $K_e(\lambda)$ and $K_e(\sigma)$) was identified. In this Part 2 paper, the "mirror image" relationship was used to derive a new σ model from the Lu et al. (2007) λ model. The new model was used to estimate σ as a function of degree of saturation using soil texture information and known σ values at dry and saturated soil conditions. Model evaluations with single and with repeated over time thermo-TDR measurements showed that the new σ model provided reliable σ estimates in soils with a unimodal particle size distribution.

Declaration of Competing Interest

The authors declare that they have no known competing financial interests or personal relationships that could have appeared to influence the work reported in this paper.

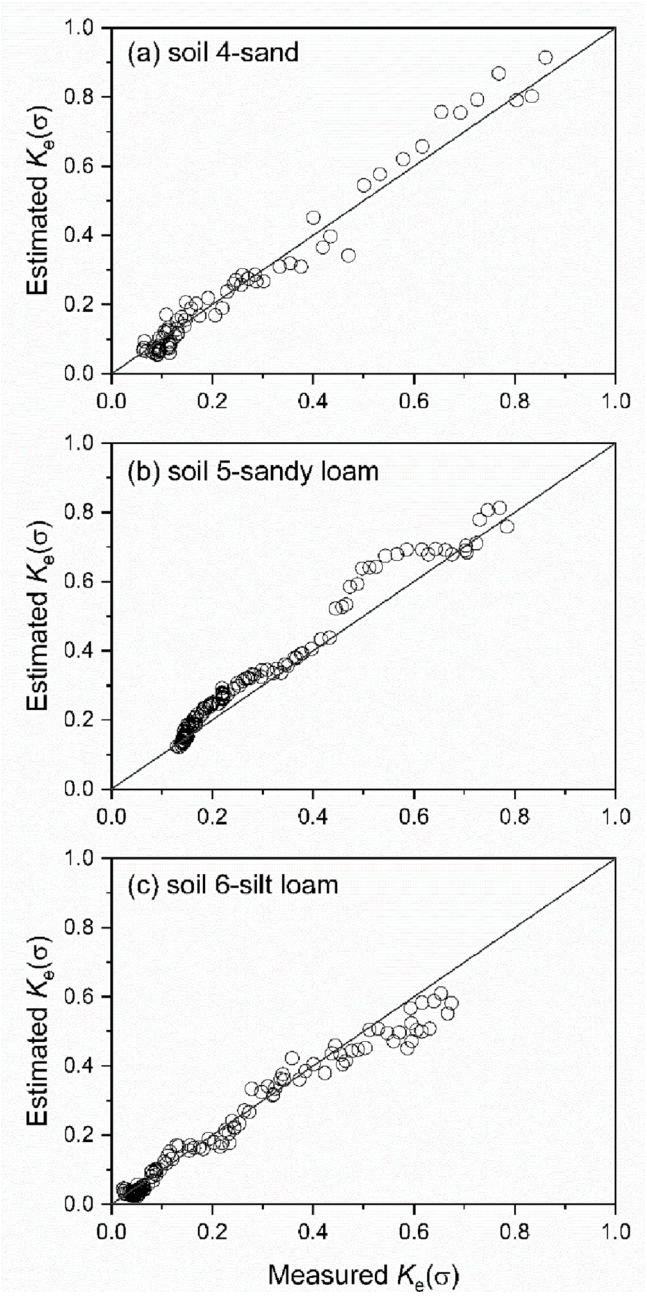

Fig. 3. Comparisons between measured and estimated normalized bulk electrical conductivity ($K_e(\sigma)$) values for soils 4–6.

Data availability

Data will be made available on request.

References

Archie, G.E., 1942. The electrical resistivity log as an aid in determining some reservoir characteristics. Trans. Am. Inst. Mining Metall. Eng. 146 (1), 54–62.

Bai, W., Kong, L., Guo, A., 2013. Effects of physical properties on electrical conductivity of compacted lateritic soil. J. Rock Mech. Geotech. Eng. 5 (5), 406–411.

Bertermann, D., Schwarz, H., 2017. Laboratory device to analyse the impact of soil properties on electrical and thermal conductivity. Int. Agrophys. 31 (2), 157–166.

Brovelli, A., Cassiani, G., 2011. Combined estimation of effective electrical conductivity and permittivity for soil monitoring. Water Resour. Res. 47 (8), W08510.

Cai, J.C., Wei, W., Hu, X.Y., Wood, D.A., 2017. Electrical conductivity models in saturated porous media: A review. Earth Sci. Rev. 171, 419–433.

Corwin, D.L., Lesch, S.M., 2005. Apparent soil electrical conductivity measurements in agriculture. Comput. Electron. Agric. 46 (1–3), 11–43.

Doolittle, J.A., Brevik, E.C., 2014. The use of electromagnetic induction techniques in soils studies. Geoderma 223–225, 33–45.

Ewing, R.P., Hunt, A.G., 2006. Dependence of the electrical conductivity on saturation in real porous media. Vadose Zone J. 5 (2), 731–741.

Farouki, O.T., 1986. Thermal Properties of Soils. Trans Tech Publication, Switzerland.

Flint, A.L., Flint, L.E., 2002. Particle density. In: Dane, J.H., Topp, G.C. (Eds.), Methods of Soil Analysis. Part. 4. Physical Methods. SSSA, Madison, WI, pp. 229–240.

Fragkogiannis, G., Apostolopoulos, G., Stamataki, S., 2010. Correlation of thermal conductivity and electrical resistivity of soil - For near surface geothermal applications. IEICE – Trans. Inf. Syst. E89-D, 1116–1119.

Fu, Y., Horton, R., Ren, T., Heitman, J.L., 2021. A general form of Archie's model for estimating bulk soil electrical conductivity. J. Hydrol. 597, 126160.

Gee, G.W., Or, D., 2002. Particle-size analysis. In: Dane, J.H., Topp, G.C. (Eds.), Methods of Soil Analysis. Part. 4. Physical Methods. SSSA Book Ser. 5. SSSA, Madison, WI, pp. 255–293.

Gerayzade, A.P., Troitskiy, N.B., Gyulalyyev, C.G., 1987. Relations between the electrophical and thermophysical characteristics of soils. Pochvovedenlye. 3, 43–47.

Globus, A.M., Arefyev, A.V., 1975. Combined investigation of the thermophysical and electrophysical properties of porous media. Pochvovedenlye. 5, 58–61.

Gupta, S.C., Hanks, R.J., 1972. Influence of water content on electrical conductivity of the Soil. Soil Sci. Soc. Am. J. 36 (6), 855–857.

Heimovaara, T.J., Focke, A.G., Bouten, W., Verstraten, J.M., 1995. Assessing temporal variations in soil water composition with time domain reflectometry. Soil Sci. Soc. Am. J. 59 (3), 689–698.

Hendrickx, J.M.H., Wraith, J.M., Corwin, D.L., Kachanoski, R.G., 2002. Solute content and concentration. In: Dane, J.H., Topp, G.C. (Eds.), Methods of Soil Analysis. Part 4. Physical Methods. SSSA, Madison, WI, pp. 1253–1321.

Johansen, O., 1975. Thermal Conductivity of Soils. Ph. diss. Norwegian University of Science and Technology, Trondheim. CRREL draft transl. 637, 1977.

Keller, G.V., 1994. Rock and mineral properties. In: Nabighian, M.N. (Ed.), Electromagnetic methods in applied geophysics. In Theory. Vol. 1. Investigations in Geophysics 3. Society of Exploration Geophysicists, Tulsa, OK, pp. 13–52.

Kitchen, N.R., Sudduth, K.A., Drummond, S.T., 1999. Soil electrical conductivity as a crop productivity measure for claypan soils. J. Prod. Agric. 12 (4), 607–617.

Knight, J.H., Kluitenberg, G.J., Kamai, T., Hopmans, J.W., 2012. Semianalytical solution for dual-probe heat-pulse applications that accounts for probe radius and heat capacity. Vadose Zone J. 11 (2).

Logsdon, S.D., Green, T.R., Bonta, J.V., Seyfried, M.S., Evett, S.R., 2010. Comparison of electrical and thermal conductivities for soils from five states. Soil Sci. 175 (12), 573–578.

Lu, Y.L., Wang, Y.J., Ren, T.S., 2013. Using late time data improves the heat-pulse method for estimating soil thermal properties with the pulsed infinite line source theory. Vadose Zone J. 12 (4), 4949–4960.

Lu, Y.L., Lu, S., Horton, R., Ren, T.S., 2014. An empirical model for estimating soil thermal conductivity from texture, water content, and bulk density. Soil Sci. Soc. Am. J. 78 (6), 1859–1868.

Lu, Y.L., Liu, X.N., Zhang, M., Heitman, J.L., Horton, R., Ren, T.S., 2017. Thermo-time domain reflectometry method: advances in monitoring in situ soil bulk density. In: Logsdon, S. (Ed.), Methods of Soil Analysis, Volume 2. Soil Science Society of America Journal, Madison, WI.

Lu, S., Ren, T.S., Gong, Y.S., Horton, R., 2007. An improved model for predicting soil thermal conductivity from water content at room temperature. Soil Sci. Soc. Am. J. 71 (1), 8–14.

Lu, S., Lu, Y.L., Peng, W., Ju, Z.Q., Ren, T.S., 2019. A generalized relationship between thermal conductivity and matric suction of soils. Geoderma 337, 491–497.

Martinez, G., Vanderlinden, K., Ordóñez, R., Muriel, J.L., 2009. Can apparent electrical conductivity improve the spatial characterization of soil organic carbon? Vadose Zone J. 8 (3), 586–593.

Mualem, Y., Friedman, S.P., 1991. Theoretical prediction of electrical conductivity in saturated and unsaturated soil. Water Resour. Res. 27 (10), 2771–2777.

Myers, D.B., Kitchen, N.R., Sudduth, K.A., Sharp, R.E., Miles, R.J., 2007. Soybean root distribution related to claypan soil properties and apparent soil electrical conductivity. Crop Sci. 47 (4), 1498–1509.

Nadler, A., Frenkel, H., 1980. Determination of soil solution electrical conductivity from bulk soil electrical conductivity measurements by the four-electrode method. Soil Sci. Soc. Am. J. 44 (6), 1216–1221.

Nelson, D.W., Sommers, L.E., 1996. Total carbon, organic carbon, and organic matter. p. 961-1010. In D.L. Sparks (ed.) Methods of Soil Analysis. Part 3. Chemical Methods. SSSA Book Series no. 5, Soil Science Society of America & American Society of Agronomy, Madison, WI.

Nocco, M.A., Ruark, M.D., Kucharik, C.J., 2018. Apparent electrical conductivity predicts physical properties of coarse soils. Geoderma 335, 1–11.

Peng, W., Lu, Y.L., Xie, X.T., Ren, T.S., Horton, R., 2019. An improved thermo-TDR technique for monitoring soil thermal properties, water content, bulk density, and porosity. Vadose Zone J. 18 (1), 190026.

Peng, W., Lu, Y.L., Wang, M.M., Ren, T.S., Horton, R., 2022. Determining water content and bulk density: The heat-pulse method outperforms the thermo-TDR method in high-salinity soils. Geoderma 407, 115564.

Ren, T.S., Noborio, K., Horton, R., 1999. Measuring soil water content, electrical conductivity, and thermal properties with a thermo-time domain reflectometry probe. Soil Sci. Soc. Am. J. 63 (3), 450–457.

Rhoades, J.D., Loveday, J., 1990. Salinity in irrigated agriculture. In: Stewart, B.A., Nielson, D.R. (Eds.), Irrigation of Agricultural Crops. Agronomy Monograph. American Society of Agronomy, Madison, WI, pp. 1089–1142.

Rhoades, J.D., Raats, P.A.C., Prather, R.J., 1976. Effects of liquid phase electrical conductivity, water content, and surface conductivity on bulk soil electrical conductivity. Soil Sci. Soc. Am. J. 40 (5), 651–655.
Rhoades, J.D., Manteghi, N.A., Shouse, P.J., Alves, W.J., 1989. Soil electrical conductivity and soil salinity: new formulations and calibrations. Soil Sci. Soc. Am. J. 53 (2), 433–439.
Satyanaga, A., Rahardjo, H., Leong, E.C., Wang, J.Y., 2013. Water characteristic curve of soil with bimodal grain-size distribution. Comput. Geotech. 48, 51–61.
Singh, D.N., Kuriyan, S.J., Manthena, K.C., 2001. A generalized relationship between soil electrical and thermal resistivities. Exp. Therm. Fluid Sci. 25 (3–4), 175–181.
Sreedeep, S., Reshma, A.C., Singh, D.N., 2005. Generalized relationship for determining soil electrical resistivity from its thermal resistivity. Therm. Fluid Sci. 29 (2), 217–226.
Stadler, A., Rudolph, S., Kupisch, M., Langensiepen, M., Kruk, J., Ewert, F., 2015. Quantifying the effects of soil variability on crop growth using apparent soil electrical conductivity measurements. Eur. J. Agron. 64, 8–20.
Sun, Q., Lv, C., 2019. Semi-empirical correlation between thermal conductivity and electrical resistivity for silt and silty clay soils. Geophysics 1–31.
Tabbagh, A., Panissod, C., Guérin, R., Cosenza, P., 2002. Numerical modeling of the role of water and clay content in soils' and rocks' bulk electrical conductivity. J. Geophys. Res. 107 (B11), 2318.
Tang, Y.B., Li, M., Bernabé, Y., Tang, H.M., Li, X.F., Bai, X.Y., Tao, Z.W., 2015. A new electrical formation factor model for bimodal carbonates: numerical studies using dual-pore percolation network. Geophys. J. Int. 201 (3), 1456–1470.
Tokoro, T., Ishikawa, T., Shirai, S., Nakamura, T., 2016. Estimation methods for thermal conductivity of sandy soil with electrical characteristics. Soils Found. 56 (5), 927–936.
Tong, B., Gao, Z., Horton, R., Li, Y., Wang, L., 2015. An empirical model for estimating soil thermal conductivity from soil water content and porosity. J. Hydrometeorol. 17 (2), 601–613.
Topp, G.C., Davis, J.L., Annan, A.P., 1980. Electromagnetic determination of soil water content: Measurements in coaxial transmission lines. Water Resour. Res. 16 (3), 574–582.
Wang, J., Zhang, X., Du, L., 2017. A laboratory study of the correlation between the thermal conductivity and electrical resistivity of soil. J. Appl. Geophys. 145, 12–16.